Multicenter three-distorted-wave approach to three-dimensional images for electron-impact-ionization dynamics of molecules: Overall agreement with experiment

Maomao Gong,[1,*] Xingyu Li,[1] Song Bin Zhang,[2] Shanshan Niu,[1] Xueguang Ren,[3,4] Enliang Wang,[3] Alexander Dorn,[3] and Xiangjun Chen[1,†]

[1]*Hefei National Laboratory for Physical Sciences at Microscale and Department of Modern Physics, University of Science and Technology of China, Hefei 230026, China*

[2]*School of Physics and Information Technology, Shaanxi Normal University, Xi'an 710119, China*

[3]*Max Planck Institute for Nuclear Physics, 69117 Heidelberg, Germany*

[4]*School of Science, Xi'an Jiaotong University, 710049 Xi'an, China*

(Received 5 July 2018; published 29 October 2018)

We report on a multicenter three-distorted-wave (MCTDW) approach to describe the electron-impact-ionization dynamics of molecules. In MCTDW, both the scattered projectile and the ejected electrons are described by distorted waves. The continuum wave functions of the incident and the two outgoing electrons are solved in the multicenter potential of neutral molecule and molecular ion, respectively. The fully differential cross section is then obtained for a given molecular orientation. Here, we present the spherically averaged triple-differential cross sections of water molecule by 81 eV electron impact. The results show good agreement with experiment in three-dimensional kinematics concerning both the angular dependence and the relative magnitude of the cross sections over a large range of analyzed angle and energy conditions.

DOI: 10.1103/PhysRevA.98.042710

I. INTRODUCTION

Atomic and molecular collision processes have played fundamental roles in the development of quantum mechanics since its early stage. In particular, electron-initiated processes are of great importance due not only to the many-body nature of the collision given ground to theoretical efforts, but also to the variety and subtlety of applications ranging from plasma physics and chemistry of planetary atmospheres to nuclear reactor technologies and ionizing radiation in medical radiation therapy [1–3]. The water molecule (H_2O) is of great interest in this regard and has attracted much attention over the years [4]. It is one of the most abundant molecules on earth and plays an important role in life science. As an example, precise cross-section data for energy depositions and angular distributions resulting from electron collisions with water are essential in charged-particle track structure analyses to model radiation damage in a biological system [5].

The full information about the ionization dynamics can be obtained in kinematically complete experiments, or so-called $(e, 2e)$ studies [6,7]. In such experiments, the energy and momenta of all final-state particles are determined, giving a triple-differential cross section (TDCS). The $(e, 2e)$ dynamics has been extensively studied experimentally as well as theoretically for a broad range of targets and kinematic conditions [8–10]. The mostly studied experimental kinematic condition is the so-called coplanar geometry in which both final-state electrons move in a plane that also contains the incoming projectile. Over the past few decades, theory has made tremendous progress in describing the electron-impact-ionization dynamics, which is now considered to be well understood for the simple atomic systems such as H and He; see, e.g., [11–15]. Moreover, electron-impact ionization of the simplest H_2 molecule has also been well described by several theoretical models even in the frame of a H_2 molecular axis; see, e.g., [16–20].

Molecular targets larger than H_2 provide a significant challenge to theory due to their multicenter nature and complex electronic structures. A key challenge in modeling electron collisions with molecules is hence in developing accurate multicenter wave functions. The ionization dynamics of water have been previously studied by the determination of TDCS [21–29]. At 250 eV impact energy, theories can nicely reproduce the binary lobe of the experimental TDCS, while there are discrepancies between theory and experiment in the recoil lobe which is originated from the nuclear backscattering process [21–25]. The situation becomes worse for results at lower impact energy, where the $(e, 2e)$ ionization dynamics are more sensitive to the effects such as postcollision interaction (PCI), exchange, and polarization [26–28].

With the emergence of the state-of-the-art reaction microscope, it became possible to image the electron emission in electron-impact ionization in all three spatial dimensions and the fully differential cross sections can be obtained for many kinematic arrangements. It thus provides benchmark experimental data of the $(e, 2e)$ process for comprehensive tests of theoretical models [29–32]. Recently, an internormalized TDCS of water has been reported at low impact energy (81 eV) using a reaction microscope [29]. It covers a large fraction of the entire solid angle and a broad range of energies of the continuum electrons in the final state. The typical molecular three-body distorted-wave (M3DW) theory [33–36]

*gongmm@mail.ustc.edu.cn
†xjun@ustc.edu.cn

has been applied to reproduce the experimental TDCS. It was found that M3DW, using a proper average (PA) over orientation-dependent cross sections, produces more accurate results than the orientation-averaged molecular orbital (OAMO) method [29]. The computational cost of the PA method, however, is much more expensive than the OAMO and therefore only the TDCS by OAMO was presented for an overall comparison in all three spatial dimensions. In our recent works, a multicenter distorted-wave (MCDW) method has been developed to calculate the $(e, 2e)$ cross sections of molecules, which is generally limited to the relatively higher impact energy (above 100 eV) and asymmetric kinematics due to the fact that the projectile was considered as a plane wave [24,37,38].

In the present work, we report a theoretical approach named multicenter three-distorted-wave method (MCTDW) to describe the single-ionization dynamics of molecules. Unlike the previous MCDW, the continuum-wave functions of incident and two outgoing electrons in MCTDW are solved under the multicenter potential of neutral molecule and molecular ion, respectively, which can be used to calculate TDCS at relatively low impact energy for all kinds of kinematics. Here, as a demonstration, three-dimensional (3D) TDCSs of water molecule as well as the cutting planes by MCTDW are compared with the internormalized cross sections of water mentioned above. We obtain an overall good agreement with the experimental data; in particular, when the PCI effect was considered in the method with a Gamow factor for the cutting planes of different kinematic conditions. When comparing at certain planes, it was found that the calculation accuracy of the MCTDW theory is at a similar level or, in some cases, better than the PA method concerning both the angular dependence and the relative magnitude of the cross sections. In particular, the low computational cost of the present approach enables us to obtain 3D TDCSs for molecular target with only dozens of processors within a couple of days.

II. THEORETICAL METHOD

A. General formulation

The electron-impact single-ionization process of a molecule (M) can be described as

$$e_0(\vec{k}_i) + M \rightarrow M^+ + e_1(\vec{k}_s) + e_2(\vec{k}_e), \tag{1}$$

where e_0, e_1, e_2 represent the incident, scattered, and ejected electrons, respectively. $\vec{k}_i$, $\vec{k}_s$, and $\vec{k}_e$ are the corresponding momentum vectors. According to the scattering theory, we can calculate the probability of the electron-scattering process quantum mechanically by evaluating a quantity called the T matrix. The transition matrix $T_{\rm fi}$ describes the transition of the scattering system from the initial stationary state Ψ_i to the final stationary state Ψ_f through the interaction potential V. In the present calculation model, approximated three-body potentials are employed,

$$V = \frac{1}{|\vec{r}_0 - \vec{r}_1|} - \frac{1}{N}\sum_n \frac{Z_n}{|\vec{r}_0 - \vec{R}_n|}. \tag{2}$$

The first term of Eq. (2) represents the interaction between the projectile and active electron, while the second term is the approximated interaction from the residual ion. $\vec{r}_0$ and $\vec{r}_1$ are the coordinates of the projectile and target active electrons. $\vec{R}_n$ is the position of the nth nucleus and Z_n indicates its charge. N is the total electron number of the molecular system. The initial and final states of the system are written as

$$\Psi_i = \psi_{\rm target}\mathcal{F}_i^{(+)}, \tag{3}$$

$$\Psi_f = \mathcal{F}_e^{(-)}\mathcal{F}_s^{(-)}\psi_{\rm ion}, \tag{4}$$

where $\psi_{\rm target}$ is the total bound wave functions of the molecular target, and $\mathcal{F}_i^{(+)}$ is the distorted wave of the incident electron in the multicenter neutral molecular potential. $\mathcal{F}_e^{(-)}$ and $\mathcal{F}_s^{(-)}$ represent the distorted waves of the ejected and scattered electrons, respectively, and will be solved in the multicenter potential of the molecular ion. $\psi_{\rm ion}$ is the total wave functions of the residual ion. So the standard T matrix gives rise to

$$T_{\rm fi}^{\rm dir}(\Omega) = \left\langle \mathcal{F}_e^{(-)}\mathcal{F}_s^{(-)}\psi_{\rm ion}\right| \frac{1}{|\vec{r}_0 - \vec{r}_1|} - \frac{1}{N}\sum_n \frac{Z_n}{|\vec{r}_0 - \vec{R}_n|}\left\langle \psi_{\rm target}\mathcal{F}_i^{(+)}\right\rangle. \tag{5}$$

The Dyson orbitals for the ionized electron can be applied,

$$\langle\psi_{\rm ion}(\{\vec{r}_2, \ldots, \vec{r}_N\})|\psi_{\rm target}(\{\vec{r}_1, \ldots, \vec{r}_N\})\rangle = \varphi_\alpha(\vec{r}_1). \tag{6}$$

Then formula (5) can further be simplified as

$$T_{\rm fi}^{\rm dir}(\Omega) = \left\langle \mathcal{F}_e^{(-)}\left(\vec{k}_e; \mathcal{R}_\Omega^{-1}\vec{r}_1\right)\mathcal{F}_s^{(-)}\left(\vec{k}_s; \mathcal{R}_\Omega^{-1}\vec{r}_0\right)\right| \frac{1}{|\vec{r}_0 - \vec{r}_1|} - \frac{1}{N}\sum_n \frac{Z_n}{|\vec{r}_0 - \vec{R}_n|}\left|\varphi_\alpha\left(\mathcal{R}_\Omega^{-1}\vec{r}_1\right)\mathcal{F}_i^{(+)}\left(\vec{k}_i; \mathcal{R}_\Omega^{-1}\vec{r}_0\right)\right\rangle. \tag{7}$$

The molecular orientation is defined by the Euler angle $\Omega = (\alpha, \beta, \gamma)$. $\mathcal{R}_\Omega^{-1}$ represents the rotation of the target. The treatment of formula (7) is very similar to the distorted-wave Born approximation (DWBA) [39,40] for an atomic system; the main difference is that we solve the distorted waves of the three electrons in the multicenter potential. Equation (7) is the direct-transition amplitude for the MCTDW model.

Since one cannot distinguish the outgoing two electrons, we have to evaluate the exchange amplitude as well,

$$T_{\rm fi}^{\rm exc}(\Omega) = \left\langle \mathcal{F}_e^{(-)}\left(\vec{k}_e; \mathcal{R}_\Omega^{-1}\vec{r}_0\right)\mathcal{F}_s^{(-)}\left(\vec{k}_s; \mathcal{R}_\Omega^{-1}\vec{r}_1\right)\right| \frac{1}{|\vec{r}_0 - \vec{r}_1|} - \frac{1}{N}\sum_n \frac{Z_n}{|\vec{r}_0 - \vec{R}_n|}\left|\varphi_\alpha\left(\mathcal{R}_\Omega^{-1}\vec{r}_1\right)\mathcal{F}_i^{(+)}\left(\vec{k}_i; \mathcal{R}_\Omega^{-1}\vec{r}_0\right)\right\rangle. \tag{8}$$

The nonrelativistic TDCS can therefore be obtained by averaging over all molecular orientations as

$$\frac{d^3\sigma}{d\Omega_e d\Omega_s dE_s} = N_e \frac{1}{(2\pi)^5}\frac{k_s k_e}{k_i}\frac{1}{8\pi^2} \times \int \left(\frac{1}{4}\left|T_{\rm fi}^{\rm dir} + T_{\rm fi}^{\rm exc}\right|^2 + \frac{3}{4}\left|T_{\rm fi}^{\rm dir} - T_{\rm fi}^{\rm exc}\right|^2\right)d\Omega, \tag{9}$$

where N_e is the electron occupation number of the ionized molecular orbital. In this standard MCTDW model, the correlation of the final two electrons is ignored. The full final-state Coulomb interaction can be included through the famous Gamow factor (N_{ee}) [41] in the expression of TDCS,

$$N_{ee} = \left|e^{-\frac{\pi\gamma}{2}}\Gamma(1-i\gamma)\right|^2 = \frac{\pi/k_{ab}}{e^{\pi/k_{ab}}-1}, \tag{10}$$

where $\Gamma(1-i\gamma)$ is the gamma function, $k_{ab} = \mu v_{ab}$, $\mu = 1/2$ is the reduced mass for the two electrons, v_{ab} is the relative velocity between the two electrons, and $\gamma = 1/v_{ab}$ is the Sommerfeld parameter.

B. Multicenter distorted waves

The wave functions of the ejected, scattered, and incident electrons can be obtained by solving the effective Schrödinger equations in the distorted or model potentials:

$$\left[-\tfrac{1}{2}\nabla^2 + V_e^m - E_{k_e}\right]\mathcal{F}^{(-)}(\vec{k_e};\vec{r_1}) = 0, \tag{11}$$

$$\left[-\tfrac{1}{2}\nabla^2 + V_s^m - E_{k_s}\right]\mathcal{F}^{(-)}(\vec{k_s};\vec{r_0}) = 0, \tag{12}$$

$$\left[-\tfrac{1}{2}\nabla^2 + V_i^m - E_{k_i}\right]\mathcal{F}^{(+)}(\vec{k_i};\vec{r_0}) = 0. \tag{13}$$

The V_e^m, V_s^m, and V_i^m are the corresponding multicenter model potentials:

$$V_{e;s;i}^m = V_{e;s;i}^{st} + V_{e;s;i}^{cp} + V_{e;s;i}^{\text{model-exc}}, \tag{14}$$

where V_s^{st}, V_e^{st} are the electrostatic potentials of the residual molecular ion for scattered and ejected electrons, while V_i^{st} is the electrostatic potential of the neutral molecule for incident electron. V_e^{cp}, V_s^{cp}, V_i^{cp} and $V_e^{\text{model-exc}}$, $V_s^{\text{model-exc}}$, $V_i^{\text{model-exc}}$ are the corresponding correlation-polarization and model exchange potentials, respectively.

In order to solve the Schrödinger equations, the single-center expansion (SCE) techniques [42–44] are employed to expand the wave functions and potentials. In order to take advantage of the point-group symmetry of the molecule, a symmetry-adapted angular function $X_{hl}^{p\mu}(\theta,\varphi)$ [42–44] was employed to do the expansion, where p and μ label one of the relevant irreducible representations and one of its components, respectively. Index h labels a specific basis, at a given angular momentum l, for the pth irreducible representations considered [42–44]. Then the continuum-wave functions of ejected, scattered, and incident electrons are obtained with the partial-wave expansion,

$$\langle\mathcal{F}^{(-)}(\vec{k_e}) \mid \vec{r_1}\rangle = \sum_{p\mu_e}\sum_{h_1\ell_1;h_2\ell_2} 4\pi i^{-\ell_1} e^{i\delta_{\ell_1}^c}\frac{1}{k_e r_1} \times f_{h_1\ell_1;h_2\ell_2}^{(-);p\mu_e}(k_e,r_1) X_{h_1\ell_1}^{p\mu_e}(\hat{k}_e) X_{h_2\ell_2}^{p\mu_e}(\hat{r}_1), \tag{15}$$

$$\langle\mathcal{F}^{(-)}(\vec{k_s}) \mid \vec{r_0}\rangle = \sum_{p\mu_s}\sum_{h_3\ell_3;h_4\ell_4} 4\pi i^{-\ell_3} e^{i\delta_{\ell_3}^c}\frac{1}{k_s r_0} \times f_{h_3\ell_3;h_4\ell_4}^{(-);p\mu_s}(k_s,r_0) X_{h_3\ell_3}^{p\mu_s}(\hat{k}_s) X_{h_4\ell_4}^{p\mu_s}(\hat{r}_0), \tag{16}$$

$$\langle\mathcal{F}^{(+)}(\vec{k_i}) \mid \vec{r_0}\rangle = \sum_{p\mu_i}\sum_{h_5\ell_5;h_6\ell_6} 4\pi i^{-\ell_5}\frac{1}{k_i r_0} \times f_{h_5\ell_5;h_6\ell_6}^{(+);p\mu_i}(k_i,r_0) X_{h_5\ell_5}^{p\mu_i}(\hat{k}_i) X_{h_6\ell_6}^{p\mu_i}(\hat{r}_0), \tag{17}$$

where $\delta_{l_{(1:3)}}^c$ is the Coulomb phase shift. The coupled equations can be obtained:

$$\left[\frac{d^2}{dr_1^2} - \frac{\ell_2(\ell_2+1)}{r_1^2} + \frac{2}{r_1} + k_e^2\right] f_{h_1\ell_1;h_2\ell_2}^{(-);p\mu_e}(k_e,r_1) = \sum_{h'\ell'} U_{h_1\ell_1;h'\ell'}^{p\mu_e}(k_e;r_1) f_{h'\ell';h_2\ell_2}^{(-);p\mu_e}(k_e,r_1), \tag{18}$$

$$\left[\frac{d^2}{dr_0^2} - \frac{\ell_4(\ell_4+1)}{r_0^2} + \frac{2}{r_0} + k_s^2\right] f_{h_3\ell_3;h_4\ell_4}^{(-);p\mu_s}(k_s,r_0) = \sum_{h'\ell'} U_{h_3\ell_3;h'\ell'}^{p\mu_s}(k_s;r_0) f_{h'\ell';h_4\ell_4}^{(-);p\mu_s}(k_s,r_0), \tag{19}$$

$$\left[\frac{d^2}{dr_0^2} - \frac{\ell_6(\ell_6+1)}{r_0^2} + k_i^2\right] f_{h_5\ell_5;h_6\ell_6}^{(+);p\mu_i}(k_i,r_0) = \sum_{h'\ell'} U_{h_5\ell_5;h'\ell'}^{p\mu_i}(k_i;r_0) f_{h'\ell';h_6\ell_6}^{(+);p\mu_i}(k_i,r_0), \tag{20}$$

where the potential matrix element is

$$U_{h_1\ell_1;h'\ell'}^{p\mu_e}(k_e;r_1) = 2\left\langle X_{h_1\ell_1}^{p\mu_e}(\hat{r}_1)\middle|V^m(k_e;\vec{r_1})\middle|X_{h'\ell'}^{p\mu_e}(\hat{r}_1)\right\rangle + \frac{2}{r_1}\delta_{h_1h'}\delta_{\ell_1\ell'}, \tag{21}$$

$$U_{h_3\ell_3;h'\ell'}^{p\mu_s}(k_s;r_0) = 2\left\langle X_{h_3\ell_3}^{p\mu_s}(\hat{r}_0)\middle|V^m(k_s;\vec{r_0})\middle|X_{h'\ell'}^{p\mu_s}(\hat{r}_0)\right\rangle + \frac{2}{r_0}\delta_{h_3h'}\delta_{\ell_1\ell'}, \tag{22}$$

$$U_{h_5\ell_5;h'\ell'}^{p\mu_i}(k_i;r_0) = 2\left\langle X_{h_5\ell_5}^{p\mu_i}(\hat{r}_0)\middle|V^m(k_i;\vec{r_0})\middle|X_{h'\ell'}^{p\mu_i}(\hat{r}_0)\right\rangle. \tag{23}$$

The coupled equations can further be written as a Volterra equation [45] and solved with the standard Green's function technique [44]. In order to solve the equation numerically, the radial wave functions $f_{h_1l_1;h_2l_2}^{(-);p\mu_e}$, $f_{h_3l_3;h_4l_4}^{(-);p\mu_s}$, and $f_{h_5l_5;h_6l_6}^{(+);p\mu_i}$ must match the physical asymptotic conditions of the K matrix [46],

$$f_{h_1l_1;h_2l_2}^{(-);p\mu_e}(k_e,r_1) \overset{r_1\to\infty}{\to} F_{l_1}(k_e r_1)\delta_{h_1l_1;h_2l_2} + G_{l_1}(k_e r_1)K_{h_1l_1;h_2l_2}^{p\mu_e}, \tag{24}$$

$$f_{h_3l_3;h_4l_4}^{(-);p\mu_s}(k_s,r_0) \overset{r_0\to\infty}{\to} F_{l_3}(k_s r_0)\delta_{h_3l_3;h_4l_4} + G_{l_3}(k_s r_0)K_{h_3l_3;h_4l_4}^{p\mu_s}, \tag{25}$$

$$f_{h_5l_5;h_6l_6}^{(+);p\mu_i}(k_i,r_0) \overset{r_0\to\infty}{\to} j_{l_5}(k_i r_0)\delta_{h_5l_5;h_6l_6} + n_{l_5}(k_i r_0)K_{h_5l_5;h_6l_6}^{p\mu_i}, \tag{26}$$

where F_l and G_l are the regular and irregular Coulomb functions, and j_l and n_l are the Riccati-Bessel and Riccati-Neumann functions. The radial wave functions for ejected and

scattered electrons satisfy the ingoing boundary condition, while the incident electron is solved with outgoing boundary condition. In the present calculations, the diagonal terms of the potential matrix are considered dominant. Thus, in practice, we will ignore the off-diagonal terms and solve the decoupled partial-wave equations.

C. Numerical process of transition amplitude

The initial bound orbital φ_α is also expanded with the symmetry-adapted angular function,

$$\varphi_\alpha(\vec{r_1}) = \frac{1}{r_1}\sum_{h_7 l_7} u_{h_7 l_7}(\vec{r_1}) X^{\alpha\mu}_{h_7 l_7}(\hat{r}_1). \tag{27}$$

Consider the expansions below,

$$\frac{1}{|\vec{r_1}-\vec{r_0}|} = \sum_{l_8 m_8}\frac{4\pi}{2l_8+1}\frac{r_<^{l_8}}{r_>^{l_8+1}} S_{l_8 m_8}(\hat{r}_1) S_{l_8 m_8}(\hat{r}_0), \tag{28}$$

$$\frac{1}{|\vec{R}_n-\vec{r_0}|} = \sum_{l_8 m_8}\frac{4\pi}{2l_8+1}\frac{r_<^{l_8}}{r_>^{l_8+1}} S_{l_8 m_8}(\hat{R}_n) S_{l_8 m_8}(\hat{r}_0), \tag{29}$$

where the $S_{l_8 m_8}$ is the real spherical harmonic function [47], $r_< = \min(r_0, r_1)$, $r_> = \max(r_0, r_1)$ or $r_< = \min(r_0, R_n)$, $r_> = \max(r_0, R_n)$. Then we can get the final expression of the transition amplitude $T_{\rm fi}(\Omega)$,

$$T_{\rm fi}(\Omega) = \mathrm{M1} - \mathrm{M2}, \tag{30}$$

where M1 and M2 are defined as

$$\mathrm{M1} \equiv \left\langle \mathcal{F}_s^{(-)}(\mathcal{R}_\Omega\vec{k}_s;\vec{r_0})\mathcal{F}_e^{(-)}(\mathcal{R}_\Omega\vec{k}_e;\vec{r_1})\right| \frac{1}{|\vec{r_0}-\vec{r_1}|}\left|\mathcal{F}_i^{(+)}(\mathcal{R}_\Omega\vec{k}_i;\vec{r_0})\varphi_\alpha(\vec{r_1})\right\rangle, \tag{31}$$

$$\mathrm{M2} \equiv \left\langle \mathcal{F}_s^{(-)}(\mathcal{R}_\Omega\vec{k}_s;\vec{r_0})\mathcal{F}_e^{(-)}(\mathcal{R}_\Omega\vec{k}_e;\vec{r_1})\right| \sum_n \frac{Z_n/N}{|\vec{r_0}-\vec{R}_n|}\left|\mathcal{F}_i^{(+)}(\mathcal{R}_\Omega\vec{k}_i;\vec{r_0})\varphi_\alpha(\vec{r_1})\right\rangle. \tag{32}$$

Then the numerical results of M1 can be expressed as

$$\begin{aligned}\mathrm{M1} = {}& \frac{(4\pi)^4}{k_e k_s k_i}\sum_{p\mu_e}\sum_{p\mu_s}\sum_{p\mu_i}\sum_{h_1 l_1}\sum_{h_3 l_3}\sum_{h_7 l_7}\sum_{h_5 l_5}\sum_{l_8 m_8}\frac{i^{-l_1-l_3+l_5}}{2l_8+1}e^{i\left(\delta^c_{l_1}+\delta^s_{l_1}+\delta^c_{l_3}+\delta^s_{l_3}-\delta^s_{l_5}\right)}\\
&\times\left[\int_0^\infty\int_0^\infty f^{p\mu_s}_{h_3 l_3}(k_s,r_0) f^{p\mu_i}_{h_5 l_5}(k_i,r_0) f^{p\mu_e}_{h_1 l_1}(k_e,r_1) u_{h_7 l_7}(r_1)\frac{r_<^{l_8}}{r_>^{l_8+1}}dr_0 dr_1\right] X^{p\mu_e}_{h_1 l_1}\left(\mathcal{R}_\Omega\hat{k}_e\right) X^{p\mu_s}_{h_3 l_3}\left(\mathcal{R}_\Omega\hat{k}_s\right) X^{p\mu_i}_{h_5 l_5}\left(\mathcal{R}_\Omega\hat{k}_i\right)\\
&\times\left[\int d\hat{r}_1 X^{p\mu_e}_{h_1 l_1}(\hat{r}_1) X^{\alpha\mu}_{h_7 l_7}(\hat{r}_1) S_{l_8 m_8}(\hat{r}_1)\right]\left[\int d\hat{r}_0 X^{p\mu_s}_{h_3 l_3}(\hat{r}_0) X^{p\mu_i}_{h_5 l_5}(\hat{r}_0) S_{l_8 m_8}(\hat{r}_0)\right],\end{aligned} \tag{33}$$

where $\delta^s_{l_{(1;3;5)}}$ is the short-range phase shift inherited from the radial wave functions $f^{(-);p\mu_e}_{h_1 l_1;h_2 l_2}$, $f^{(-);p\mu_s}_{h_3 l_3;h_4 l_4}$, and $f^{(+);p\mu_i}_{h_5 l_5;h_6 l_6}$. For M2, if $\vec{R}_n = 0$, then

$$\begin{aligned}\mathrm{M2} = {}& \frac{(4\pi)^4}{k_e k_s k_i}\sum_n\frac{Z_n}{N_e}\left\{\sum_{p\mu_e}\sum_{h_1 l_1}\sum_{h_7 l_7} i^{-l_1}e^{i\left(\delta^c_{l_1}+\delta^s_{l_1}\right)}\left[\int_0^\infty dr_1 f^{p\mu_e}_{h_1 l_1}(k_e,r_1)u_{h_7 l_7}(r_1)\right]\left[\int d\hat{r}_1 X^{p\mu_e}_{h_1 l_1}(\hat{r}_1)X^{\alpha\mu}_{h_7 l_7}(\hat{r}_1)\right]X^{p\mu_e}_{h_1 l_1}\left(\mathcal{R}_\Omega\hat{k}_e\right)\right\}\\
&\times\left\{\sum_{p\mu_s}\sum_{p\mu_i}\sum_{h_3 l_3}\sum_{h_5 l_5} i^{-l_3+l_5}e^{i\delta^c_{l_3}+i\delta^s_{l_3}-i\delta^s_{l_5}}\left[\int_0^\infty dr_0 f^{p\mu_s}_{h_3 l_3}(k_s,r_0) f^{p\mu_i}_{h_5 l_5}(k_i,r_0)/r_0\right]\right.\\
&\left.\times\left[\int d\hat{r}_0 X^{p\mu_s}_{h_3 l_3}(\hat{r}_0)X^{p\mu_i}_{h_5 l_5}(\hat{r}_0)\right]X^{p\mu_s}_{h_3 l_3}\left(\mathcal{R}_\Omega\hat{k}_s\right)X^{p\mu_i}_{h_5 l_5}\left(\mathcal{R}_\Omega\hat{k}_i\right)\right\}.\end{aligned} \tag{34}$$

If $\vec{R}_n \neq 0$, then

$$\begin{aligned}\mathrm{M2} = {}& \frac{(4\pi)^4}{k_e k_s k_i}\sum_n\frac{Z_n}{N_e}\left\{\sum_{p\mu_e}\sum_{h_1 l_1}\sum_{h_7 l_7} i^{-l_1}e^{i\left(\delta^c_{l_1}+\delta^s_{l_1}\right)}\left[\int_0^\infty dr_1 f^{p\mu_e}_{h_1 l_1}(k_e,r_1)u_{h_7 l_7}(r_1)\right]\left[\int d\hat{r}_1 X^{p\mu_e}_{h_1 l_1}(\hat{r}_1)X^{\alpha\mu}_{h_7 l_7}(\hat{r}_1)\right]X^{p\mu_e}_{h_1 l_1}\left(\mathcal{R}_\Omega\hat{k}_e\right)\right\}\\
&\times\left\{\sum_{p\mu_s}\sum_{p\mu_i}\sum_{h_3 l_3}\sum_{l_5 m_5}\sum_{l_8 m_8}\frac{i^{-l_3+l_5}}{2l_8+1}e^{i\delta^c_{l_3}+i\delta^s_{l_3}-i\delta^s_{l_5}}\left[\int_0^\infty dr_0 f^{p\mu_s}_{h_3 l_3}(k_s,r_0) f^{p\mu_i}_{h_5 l_5}(k_i,r_0)\frac{r_<^{l_8}}{r_>^{l_8+1}}\right]\right.\\
&\left.\times\left[\int d\hat{r}_0 X^{p\mu_s}_{h_3 l_3}(\hat{r}_0)X^{p\mu_i}_{h_5 l_5}(\hat{r}_0)S_{l_8 m_8}(\hat{r}_0)\right]X^{p\mu_s}_{h_3 l_3}\left(\mathcal{R}_\Omega\hat{k}_s\right)X^{p\mu_i}_{h_5 l_5}\left(\mathcal{R}_\Omega\hat{k}_i\right)S_{l_8 m_8}\left(\mathcal{R}_\Omega\hat{R}_n\right)\right\}.\end{aligned} \tag{35}$$

For the radial integration of M1, it is hard to achieve convergence due to the large radial scale of continuum-wave functions. Let R_{M1} denotes the final result of radial integration of M1,

$$R_{M1} = \int_0^\infty\int_0^\infty f^{p\mu_s}_{h_3 l_3}(k_s,r_0) f^{p\mu_i}_{h_5 l_5}(k_i,r_0) f^{p\mu_e}_{h_1 l_1}(k_e,r_1) u_{h_7 l_7}(r_1)\frac{r_<^{l_8}}{r_>^{l_8+1}}dr_0 dr_1. \tag{36}$$

The radial bound wave function $u_{l_7 m_7}(r_1)$ will approach to zero when r_1 is larger than R_0,

$$u_{h_7 l_7}(r_1) \overset{r_1 \geqslant R_0}{\rightarrow} 0, \tag{37}$$

where R_0 is defined as the critical integration point. Then the following radial integration expression can be obtained:

$$R_{M1} = \int_0^{R_0} dr_0 f^{p\mu_s}_{h_3 l_3}(k_s, r_0) f^{p\mu_i}_{h_5 l_5}(k_i, r_0) \left[\int_0^{r_0} dr_1 f^{p\mu_e}_{h_1 l_1}(k_e, r_1) u_{h_7 l_7}(r_1) \frac{r_1^{l_8}}{r_0^{l_8+1}} + \int_{r_0}^{R_0} dr_1 f^{p\mu_e}_{h_1 l_1}(k_e, r_1) u_{h_7 l_7}(r_1) \frac{r_0^{l_8}}{r_1^{l_8+1}} \right]$$
$$+ \int_{R_0}^{\infty} dr_0 f^{p\mu_s}_{h_3 l_3}(k_s, r_0) f^{p\mu_i}_{h_5 l_5}(k_i, r_0) \int_0^{R_0} dr_1 f^{p\mu_e}_{h_1 l_1}(k_e, r_1) u_{h_7 l_7}(r_1) \frac{r_1^{l_8}}{r_0^{l_8+1}}. \tag{38}$$

After testing the program, when the critical integration point $R_0 \geqslant 30$ a.u., TDCS could achieve a good convergence. In practice, we use $R_0 = 40$ a.u. to do the calculations.

In the present work, the bound wave functions of the molecular orbitals (MOs) of H_2O are calculated using the GAUSSIAN 09 [48] program with the density functional theory employing the B3LYP functional and cc-pVTZ basis set. For the present calculation of H_2O, let $l^b_{\max}$, $l^e_{\max}$, $l^s_{\max}$, and $l^i_{\max}$ denote the upper limits of the angular momentum in the partial-wave expansions for the bound orbital, continuum-wave functions of ejected, scattering, and incident electrons, respectively. Convergence is achieved with up limits $l^b_{\max} = 2$, $l^e_{\max} = 6$, $l^s_{\max} = 35$, and $l^i_{\max} = 40$. The spherical average of cross sections for different molecular orientations is completed with Euler angle mesh $N_\alpha = 8$, $N_\beta = 6$, and $N_\gamma = 8$, where N_α, N_β, and N_γ represent the number of points for Euler angle α, β, and γ.

III. RESULTS AND DISCUSSION

Figure 1 presents the summed TDCSs for the ionization of $1b_1$ and $3a_1$ orbitals of the water molecule by 81 eV electron impact as three-dimensional (3D) surface plots for a projectile scattering angle of $\theta_s = -10^\circ$ as a function of the emission direction of a slow ejected electron with $E_e = 10$ eV energy. Figure 1(a) corresponds to the calculated result by the present MCTDW, while Fig. 1(b) shows the experimental data reported in [29]. The projectile ($\vec{k}_i$) enters from the bottom and is scattered ($\vec{k}_s$) to the left. These two vectors, whose intersection corresponds to the collision point, define the scattering plane, as indicated by the solid (red) frame in Fig. 1(a). In the 3D plots, the TDCS for a particular direction is defined as the distance from the origin to the surface of the plot. The momentum transfer to the target is indicated by the arrow labeled $\vec{q}$. The 3D image shows a typical two-lobe structure: one is the well-known binary lobe which is located roughly around the direction of momentum-transfer vector $\vec{q}$ and, in the opposite direction, a recoil lobe can be found. The binary lobe can be explained as the binary collision between the projectile and target electrons, while the recoil lobe results from the backscattering of the ejected electron by the ionic potential. Regarding the comparison between theory and experiment, the observed features in the 3D image are very well reproduced by theory, except that the experimental binary lobe shows a slight minimum roughly in the direction of $\vec{q}$, while it is more flat in the theory. Such a minimum or dip in the binary lobe might be the result of the characteristic momentum profile of the p-type $1b_1$ and $3a_1$ orbitals of H_2O that has a node for vanishing momentum [29].

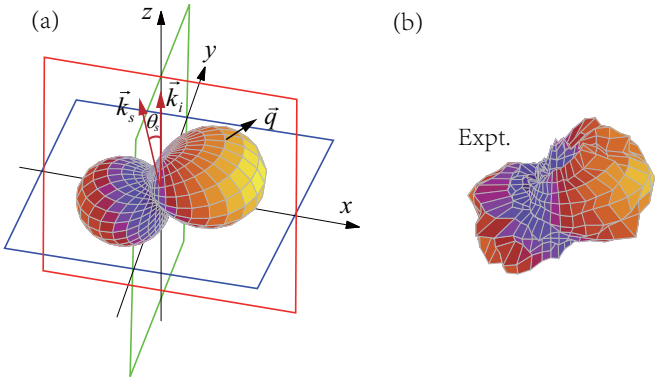

FIG. 1. (a) The 3D image is the MCTDW calculation of the low-impact-energy (81 eV) summed TDCSs for $1b_1$ and $3a_1$ orbitals of H_2O at $\theta_s = -10^\circ$ and $E_e = 10$ eV. (b) The corresponding experimental data carried out with an advanced reaction microscope [29].

In order to have a complete and comprehensive comparison, the cross sections in three orthogonal planes are presented in Figs. 2 and 3. Those are the xz plane or scattering plane, the yz plane or half-perpendicular plane, and the xy plane or full-perpendicular plane, which are cuts through the 3D image as indicated in Fig. 1(a). The studied kinematics are (i) $E_e = 5$ eV, $\theta_s = -6^\circ$; (ii) $E_e = 10$ eV, $\theta_s = -6^\circ$; (iii) $E_e = 5$ eV, $\theta_s = -10^\circ$, and (iv) $E_e = 10$ eV, $\theta_s = -10^\circ$, as presented in the panels from top to bottom in Figs. 2 and 3. Since the experimental data are internormalized for different kinematical situations [29], a single common scaling factor is sufficient to fix the relative magnitude of the experimental and theoretical data for all cases. The global scaling factor is obtained by achieving a good visual fit of experiment and the MCTDW calculations for the TDCS in the xy plane at $\theta_s = -10^\circ$ and $E_e = 10$ eV [Fig. 2(d)]. This factor is subsequently applied to all other kinematics and planes. As can be seen in Figs. 2(a)–2(d), which show the TDCS data in the full-perpendicular plane or xy plane, the MCTDW calculations are in good agreement with the experimental data both in shape and magnitude.

Figures 2(e)–2(h) show the results of TDCSs for the ejected electron in the scattering plane, i.e., xz plane. The momentum-transfer vector $\vec{q}$ lies in this plane, which is

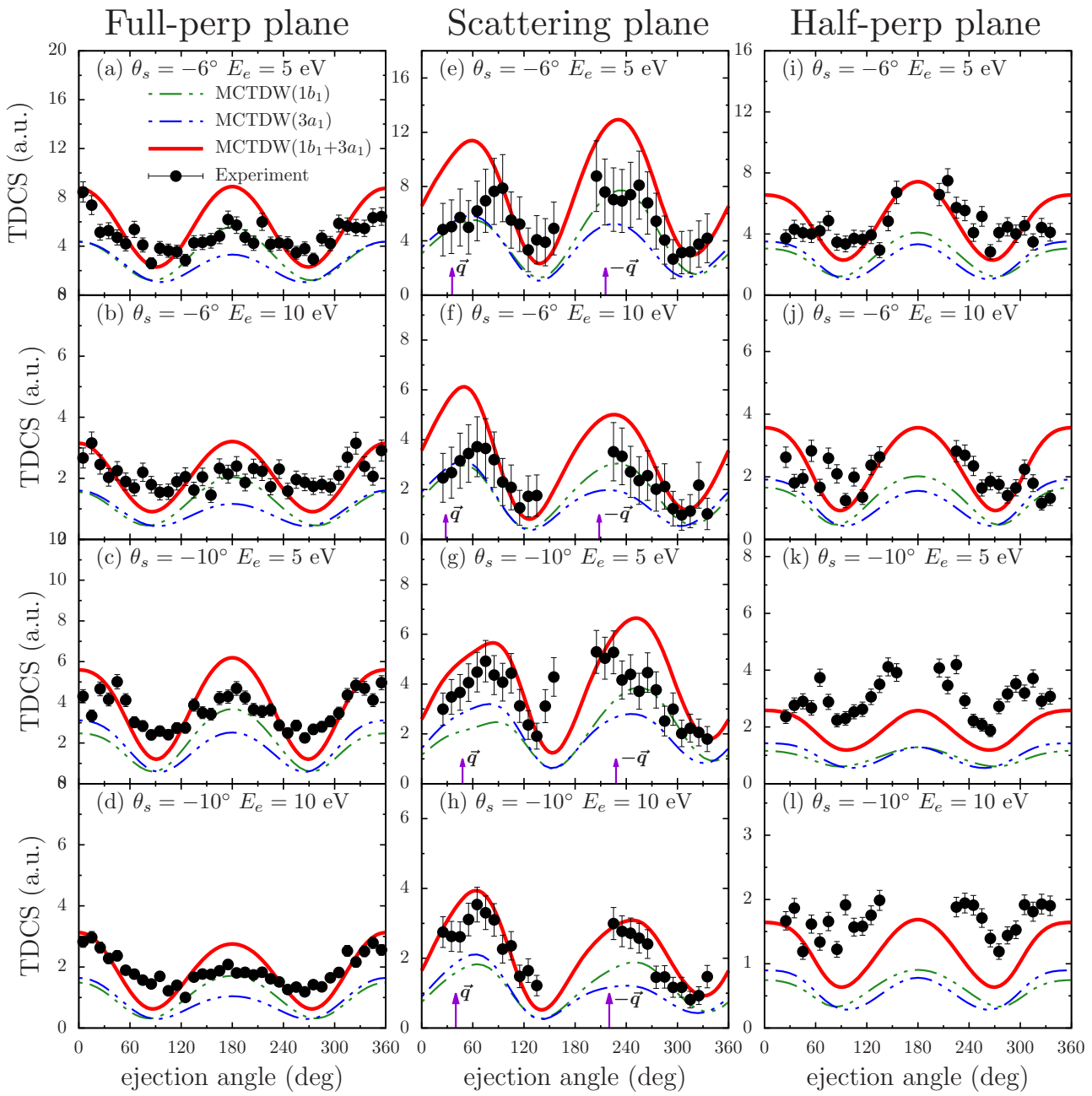

FIG. 2. TDCSs for electron-impact ionization of $1b_1$ and $3a_1$ orbitals of H_2O under asymmetric kinematics. The incident electron energy is 81 eV. The panels, from top to bottom (four rows), correspond to four conditions: $\theta_s = -6°$, $E_e = 5$ eV; $\theta_s = -6°$, $E_e = 10$ eV; $\theta_s = -10°$, $E_e = 5$ eV; $\theta_s = -10°$, $E_e = 10$ eV. The panels, from left to right (three columns), correspond to three cutting planes in the 3D image of TDCS: full-perpendicular plane (xy plane), scattering plane (xz plane), and half-perpendicular plane (yz plane). The red solid line is the summed TDCS of $1b_1$ and $3a_1$ orbitals for MCTDW results and the green and blue dashed lines are the corresponding TDCS of $1b_1$ and $3a_1$ orbitals. The circle points are the experimental data reported by Ren *et al.* [29].

indicated by an arrow. The binary peak of the MCTDW calculations is not symmetric about the momentum-transfer direction, which is evidence of the calculation beyond the first Born approximation [37,38]. In Figs. 2(e) and 2(f), the binary peaks of the MCTDW calculations have an obvious shift to the small ejection angle compared with the experimental data. This may result from the PCI effect, which is not included in the MCTDW calculations. In addition, the present MCTDW calculations overestimate the binary peak of the experiment for $\theta_s = -6°$. For $\theta_s = -10°$, shown in Figs. 2(g) and 2(h), however, the shift of the binary peaks from the experimental data disappears. Meanwhile, better agreement between the calculation and the experiment has been achieved for the binary peaks. The experimental results in the xz plane for all four kinematic conditions exhibit very strong recoil peaks in the $-\vec{q}$ direction. MCTDW calculations well reproduce the experiments both in shape and internormalized magnitude in this plane.

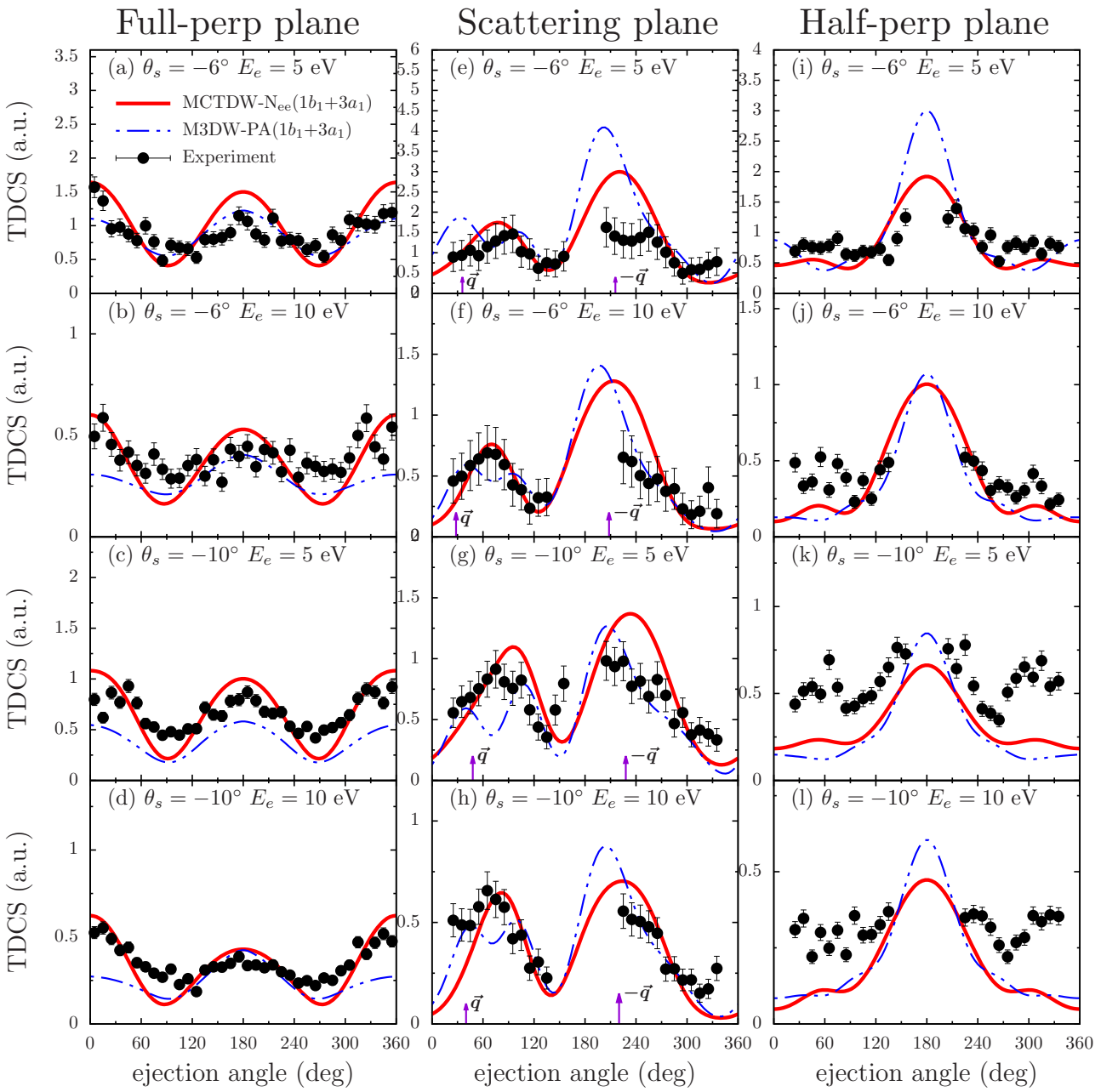

FIG. 3. Same as in Fig. 2, but the red solid line represents the MCTDW-N_{ee} calculation, and the blue dashed line is the reported calculation of M3DW-PA [29].

Figures 2(i)–2(l) compare the MCTDW results with the experimental data in the half-perpendicular plane, i.e., the yz plane. The TDCSs have bilateral symmetry about 180°, which is illustrated in both MCTDW calculations and experimental measurements. The MCTDW calculations reproduce the experiments with a maximum at 180° and two minimums located approximately at 90° and 270°, but generally overestimate the TDCSs near 0° and 360° where two outgoing electrons are emitted with the smallest intersection angle. This deviation may also be attributed to the PCI effect.

As we have mentioned, the PCI effect is not included in the present MCTDW calculations. In order to investigate the influence of PCI on the TDCSs of the H_2O molecule, we have carried out MCTDW-N_{ee} calculations where the PCI effect is taken into account by the Gamow factor [41]. The results are displayed in Fig. 3. The normalization is in the same way as in Fig. 2. The calculations based on the M3DW-PA model [29] are also presented for comparison. The improvements in reproducing experiments for the present calculations for all cases have been achieved compared with the M3DW-PA results, especially for the binary peaks in the xz plane in both shape and peak position, which confirms the importance of the PCI effect in the low-energy ionization situation. But the MCTDW-N_{ee} still overestimates the TDCSs ranging from ∼90°-270° for $\theta_s = -6°$ in the recoil region in the xz plane, while it underestimates those in the region of ∼0°-90° and ∼ 270°-360° for $\theta_s = -10°$ in the yz plane. Regarding the complexity of the H_2O molecule, the final

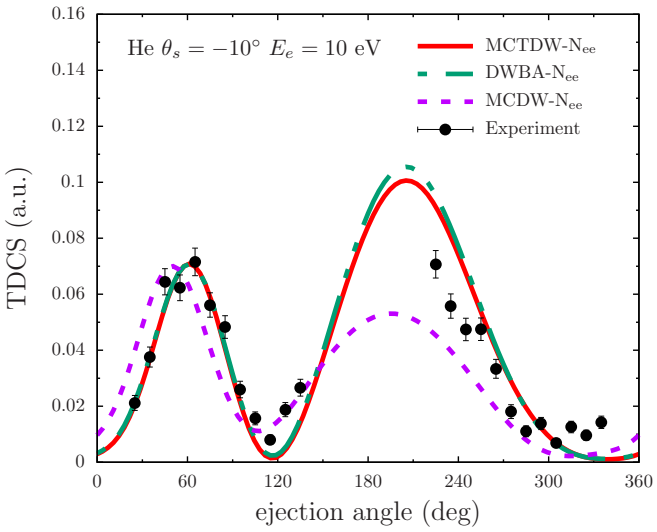

FIG. 4. The comparison of low-impact-energy (81 eV) TDCS for He at $E_e = 10$ eV, $\theta_s = -10°$ for the DWBA-N_{ee} (green short-long dashed line), MCTDW-N_{ee} (red solid line), and MCDW-N_{ee} models (purple dashed line), and the experimental data (circle point).

state with the Gamow factor may not be precise enough to describe the fully correlated two-electron wave function in the three-center ion.

The MCTDW method aims at developing a universal calculation model in treating the $(e, 2e)$ process for atoms and molecules in the perturbative framework. It can also be regarded as an upgrade of the traditional DWBA [39,40] method to some extent, although the details of the theoretical treatment are different. They should be at the same calculation level for an atomic system. Here, we also present the theoretical calculations by DWBA-N_{ee}, MCTDW-N_{ee}, and MCDW-N_{ee} [24] with the experimental results of the He atom at the kinematic conditions of $E_i = 81$ eV, $\theta_s = -10°$, and $E_e = 10$ eV, which were measured simultaneously in the experiment of H_2O [29]. The TDCS distribution as a function of ejection angle for He in the scattering plane is displayed in Fig. 4. DWBA-N_{ee} and MCTDW-N_{ee} models predict nearly the same TDCS distributions, both well reproducing the experiment, while MCDW-N_{ee} significantly underestimates the intensity of the recoil peak. The good agreement between MCTDW-N_{ee}, DWBA-N_{ee}, and the experimental data demonstrates the precision and generality of the present MCTDW model.

IV. SUMMARY

In conclusion, a multicenter three-distorted-wave method is developed to study the single-ionization dynamics of molecules in the perturbative framework. Due to the relatively low computational cost, this method can be used to calculate the 3D-TDCS of a molecule generally for any kinematic arrangement. As one example, the 3D-TDCS for H_2O molecule at kinematic condition $E_i = 81$ eV, $\theta_s = -10°$, and $E_e = 10$ eV is calculated. Good agreement is achieved between the present calculation and the recent experiment by reaction microscope [29]. In order to have a complete and comprehensive test of the present theoretical approach, MCTDW and MCTDW-N_{ee} calculations are performed in three cutting planes (xy, xz, and yz plane) for four different kinematics. The results show an overall good agreement with the experiment using one normalization factor. The precision and generality of MCTDW is also demonstrated in the case of He atom at the same incident energy. Both the studies of H_2O and He indicate that the present MCTDW approach can accurately reproduce the $(e, 2e)$ cross sections in the low-collision energy for both atoms and complex molecules.

ACKNOWLEDGMENTS

This work is supported by the National Natural Science Foundation of China (Grants No. 11534011 and No. 11774281) and the National Key Research and Development Program of China under Grant No. 2017YFA0402300. S.B.Z. and X.R. acknowledge the Project of Thousand Youth Talents in China. E.W. is grateful for a fellowship from the Alexander von Humboldt Foundation. The numerical calculations in this paper have been done on the supercomputing system in the Supercomputing Center of University of Science and Technology of China.

[1] K. Bartschat and M. J. Kushner, Proc. Natl. Acad. Sci. **113**, 7026 (2016).
[2] E. Alizadeh, T. M. Orlando, and L. Sanche, Annu. Rev. Phys. Chem **66**, 379 (2015).
[3] I. Baccarelli, I. Bald, F. A. Gianturco, E. Illenberger, and J. Kopyra, Phys. Rep. **508**, 1 (2011).
[4] B. C. Garrett *et al.*, Chem. Rev. **105**, 355 (2005).
[5] M. Bernal *et al.*, Phys. Med. **31**, 861 (2015).
[6] H. Ehrhardt, M. Schulz, T. Tekaat, and K. Willmann, Phys. Rev. Lett. **22**, 89 (1969).
[7] U. Amaldi, A. Egidi, R. Marconero, and G. Pizzella, Rev. Sci. Instrum. **40**, 1001 (1969).
[8] H. Ehrhardt, K. Jung, G. Knoth, and P. Schlemmer, Z. Phys. D: At. Mol. Clust. **1**, 3 (1986).
[9] A. Lahmam-Bennani, J. Phys. B: At. Mol. Opt. Phys. **24**, 2401 (1991).
[10] D. H. Madison and O. Al-Hagan, J. At. Mol. Opt. Phys. **2010**, 367180 (2010).
[11] T. N. Rescigno, M. Baertschy, W. A. Isaacs, and C. W. McCurdy, Science **286**, 2474 (1999).
[12] I. Bray, D. Fursa, A. Kadyrov, A. Stelbovics, A. Kheifets, and A. Mukhamedzhanov, Phys. Rep. **520**, 135 (2012).
[13] X. Ren, A. Senftleben, T. Pflüger, K. Bartschat, O. Zatsarinny, J. Berakdar, J. Colgan, M. S. Pindzola, I. Bray, D. V. Fursa, and A. Dorn, Phys. Rev. A **92**, 052707 (2015).
[14] O. Zatsarinny and K. Bartschat, Phys. Rev. Lett. **107**, 023203 (2011).
[15] X. Ren, A. Senftleben, T. Pflüger, A. Dorn, J. Colgan, M. S. Pindzola, O. Al-Hagan, D. H. Madison, I. Bray, D. V. Fursa, and J. Ullrich, Phys. Rev. A **82**, 032712 (2010).
[16] O. Al-Hagan, C. Kaiser, D. Madison, and A. J. Murray, Nat. Phys. **5**, 59 (2009).

[17] X. Ren, T. Pflüger, S. Xu, J. Colgan, M. S. Pindzola, A. Senftleben, J. Ullrich, and A. Dorn, Phys. Rev. Lett. **109**, 123202 (2012).
[18] J. Colgan, M. S. Pindzola, F. Robicheaux, C. Kaiser, A. J. Murray, and D. H. Madison, Phys. Rev. Lett. **101**, 233201 (2008).
[19] M. C. Zammit, J. S. Savage, D. V. Fursa, and I. Bray, Phys. Rev. Lett. **116**, 233201 (2016).
[20] X. Li, X. Ren, K. Hossen, E. Wang, X. Chen, and A. Dorn, Phys. Rev. A **97**, 022706 (2018).
[21] D. S. Milne-Brownlie, S. J. Cavanagh, B. Lohmann, C. Champion, P. A. Hervieux, and J. Hanssen, Phys. Rev. A **69**, 032701 (2004).
[22] C. Champion, C. Dal Cappello, S. Houamer, and A. Mansouri, Phys. Rev. A **73**, 012717 (2006).
[23] I. Tóth, R. I. Campeanu, and L. Nagy, Eur. Phys. J. D **66**, 21 (2012).
[24] S. B. Zhang, X. Y. Li, J. G. Wang, Y. Z. Qu, and X. Chen, Phys. Rev. A **89**, 052711 (2014).
[25] C.-Y. Lin, C. W. McCurdy, and T. N. Rescigno, Phys. Rev. A **89**, 012703 (2014).
[26] C. Kaiser, D. Spieker, J. Gao, M. Hussey, A. Murray, and D. H. Madison, J. Phys. B: At. Mol. Opt. Phys. **40**, 2563 (2007).
[27] K. L. Nixon, A. J. Murray, O. Al-Hagan, D. H. Madison, and C. Ning, J. Phys. B: At. Mol. Opt. Phys. **43**, 035201 (2010).
[28] M. Sahlaoui, M. Bouamoud, B. Lasri, and M. Dogan, J. Phys. B: At. Mol. Opt. Phys. **46**, 115206 (2013).
[29] X. Ren, S. Amami, K. Hossen, E. Ali, C. G. Ning, J. Colgan, D. Madison, and A. Dorn, Phys. Rev. A **95**, 022701 (2017).
[30] T. Pflüger, O. Zatsarinny, K. Bartschat, A. Senftleben, X. Ren, J. Ullrich, and A. Dorn, Phys. Rev. Lett. **110**, 153202 (2013).
[31] X. Ren, S. Amami, O. Zatsarinny, T. Pflüger, M. Weyland, W. Y. Baek, H. Rabus, K. Bartschat, D. Madison, and A. Dorn, Phys. Rev. A **91**, 032707 (2015).
[32] X. Ren, S. Amami, O. Zatsarinny, T. Pflüger, M. Weyland, A. Dorn, D. Madison, and K. Bartschat, Phys. Rev. A **93**, 062704 (2016).
[33] J. D. Builth-Williams *et al.*, J. Chem. Phys. **139**, 034306 (2013).
[34] J. D. Builth-Williams *et al.*, J. Chem. Phys. **140**, 214312 (2014).
[35] G. B. da Silva *et al.*, J. Chem. Phys. **141**, 124307 (2014).
[36] D. B. Jones *et al.*, J. Chem. Phys. **145**, 164306 (2016).
[37] X. Li, M. Gong, L. Liu, Y. Wu, J. Wang, Y. Qu, and X. Chen, Phys. Rev. A **95**, 012703 (2017).
[38] M. Gong, X. Li, S. B. Zhang, L. Liu, Y. Wu, J. Wang, Y. Qu, and X. Chen, Phys. Rev. A **96**, 042703 (2017).
[39] D. H. Madison, R. V. Calhoun, and W. N. Shelton, Phys. Rev. A **16**, 552 (1977).
[40] I. E. McCarthy, Aust. J. Phys. **48**, 1 (1995).
[41] S. J. Ward and J. H. Macek, Phys. Rev. A **49**, 1049 (1994).
[42] N. Sanna and F. Gianturco, Comput. Phys. Commun. **128**, 139 (2000).
[43] N. Sanna and G. Morelli, Comput. Phys. Commun. **162**, 51 (2004).
[44] N. Sanna, I. Baccarelli, and G. Morelli, Comput. Phys. Commun. **180**, 2544 (2009).
[45] T. A. Burton, *Volterra Integral and Differential Equations (Mathematics in Science and Engineering)*, 2nd ed. (Elsevier Science, New York, 2005).
[46] P. G. Burke, *R-Matrix Theory of Atomic Collisions*, Springer Series on Atomic, Optical and Plasma Physics (Springer, Berlin, 2011), Vol. 61.
[47] H. H. Homeier and E. Steinborn, J. Mol. Struct: THEOCHEM **368**, 31 (1996).
[48] M. J. Frisch, G. W. Trucks, H. B. Schlegel, G. E. Scuseria, M. A. Robb, J. R. Cheeseman, G. Scalmani, V. Barone, G. A. Petersson, H. Nakatsuji *et al.*, Gaussian 09, Revision A.02, Technical Report.